Environmental Science and Pollution Research (2020) 27:44089–44105
https://doi.org/10.1007/s11356-020-10166-8

RESEARCH ARTICLE

Synthesis and characterization of magnetic clay-based carboxymethyl cellulose-acrylic acid hydrogel nanocomposite for methylene blue dye removal from aqueous solution

Nompumelelo Malatji[1] · Edwin Makhado[1] · Kabelo Edmond Ramohlola[1] · Kwena Desmond Modibane[1] · Thabiso Carol Maponya[1] · Gobeng Release Monama[1] · Mpitloane Joseph Hato[1]

Received: 28 March 2020 / Accepted: 16 July 2020 / Published online: 5 August 2020

Abstract

Carboxymethyl cellulose/poly(acrylic acid) (CMC-cl-pAA) hydrogel and its magnetic hydrogel nanocomposite (CMC-cl-pAA/Fe_3O_4-C30B) were prepared via a free radical polymerization method and used as adsorbents for adsorption of methylene blue (MB) dye. The samples were characterized using Fourier transform infrared, X-ray diffraction, thermogravimetric analysis, scanning electron microscopy coupled with energy-dispersive X-ray spectrometer, high-resolution transmission electron microscope, and dynamic mechanical analysis. The adsorption performance of the prepared adsorbents was studied in a batch mode. Adsorption kinetics and isotherm models were applied in the experimental data to evaluate the nature as well as the mechanism of adsorption processes. It was deduced that the adsorption followed the pseudo-second-order rate equation and Langmuir isotherm models. The maximum adsorption capacities were found to be 1109.55 and 1081.60 mg/g for CMC-cl-pAA hydrogel and CMC-cl-pAA/Fe_3O_4-C30B hydrogel nanocomposite, respectively. The adsorption thermodynamic studies suggested that the adsorption process was spontaneous and endothermic for CMC-cl-pAA/Fe_3O_4-C30B hydrogel nanocomposite. The homogeneous dispersion of the Fe_3O_4-C30B nanocomposite in the CMC-cl-pAA hydrogel significantly improved the thermal stability, mechanical strength, and excellent regeneration stability. This study demonstrates the application potential of the fascinating properties of CMC-cl-pAA/Fe_3O_4-C30B hydrogel nanocomposite as a highly efficient adsorbent in the removal of organic dyes from aqueous solution.

Keywords Carboxymethyl cellulose · Polymerization · Hydrogel nanocomposite · Thermomechanical properties · Methylene blue · Adsorption behaviour

Introduction

In recent years, the rapid industrialization has amounted to a rise in dye-containing industrial effluents. Industries such as textile, paper printing, leather, food, and cosmetics contribute large amounts of wastewater laden containing dyes (Thakur et al. 2016). Methylene blue (MB) dye is a commonly used dye in the aforementioned industries. This dye has a planar and complex structure which is responsible for its stubbornness to be removed from water (Liu et al. 2018). It is reported that the exposure and indigestion of MB dye may cause health problems such as vomiting, nausea, eye burn, and breathing difficulties in humans, even at low concentration (Thakur et al. 2016). Its accumulation in water may inhibit the penetration of sunlight, thus hindering photosynthesis from taking place (Zhang et al. 2014; Toor et al. 2006). Various techniques

Responsible Editor: Angeles Blanco

Electronic supplementary material The online version of this article (https://doi.org/10.1007/s11356-020-10166-8) contains supplementary material, which is available to authorized users.

✉ Edwin Makhado
edwinmakhado@yahoo.com

✉ Kwena Desmond Modibane
kwena.modibane@ul.ac.za

✉ Mpitloane Joseph Hato
mpitloane.hato@ul.ac.za

[1] Nanotechnology Research Lab, Department of Chemistry, School of Physical and Mineral Sciences, University of Limpopo (Turfloop), Sovenga, 0727 Polokwane, South Africa

for water remediation such as chemical oxidation, coagulation and flocculation, membrane filtration, and adsorption have been employed to remove dyes from aqueous solution (Adegoke and Bello 2015). Amongst these techniques, the adsorption method has been reported to be a promising technique in the removal of dyes owing to its easy operation, low cost, and easy design (Yagub et al. 2014). Several materials have been applied in the adsorption of dyes from an aqueous solution, such as fly ash, activated carbon, graphene oxide, and multiwalled carbon nanotubes (Geçgel et al. 2016; Sulistiyo et al. 2017; Zhao and Yang 2017). However, these materials have high operational cost, partial removal of dyes, and non-biodegradability (Boumediene et al. 2018; De Gisi et al. 2016). For this reason, a great focus has been on the development of ideal adsorbent materials which are effective, inexpensive, easily available, and environmentally friendly.

Hydrogels are cross-linked polymer chains that can trap fluids for a longer period, and are hydrophilic in nature (Makhado et al. 2019a, b, c). For this reason, hydrogels are used in various fields such as agriculture, drug delivery, diapers, and adsorbent material (Makhado et al. 2019a, b, c). The application of polysaccharide-based hydrogels as adsorbents offers several advantages such as high adsorption efficiency, recovery capacities, and biodegradability (Shi et al. 2013). Various polysaccharides that have been used to prepare hydrogels include cellulose, alginate, chitosan, chitin, xanthan gum, and carrageenan (Makhado et al. 2019a, b, c).

Carboxymethyl cellulose (CMC) is an important water-soluble biopolymer cellulose derivative, and a linear polysaccharide produced by the chemical modification of cellulose (Yadav et al. 2013). It is a negatively charged polyelectrolyte polysaccharide that behaves as a polyanion at pH greater than 4.5 (Peng et al. 2016). Owing to its biodegradability, biocompatibility, and non-toxic nature, CMC has been used in various fields such as environmental, industrial, and biomedical fields (Kono 2014; Dai et al. 2018). The use of CMC in wastewater treatment is due to its high degree of hydrophilicity and non-toxicity (Peng et al. 2016; Godiya et al. 2018). However, poor mechanical strength and water solubility limit its practical applicability as an adsorbent (Peng et al. 2016). In this concern, it is worth mentioning that the functionalization of CMC with synthetic polymers provides desirable properties which can improve mechanical strength and adsorption capacity (Hoffman 2012).

Recently, several researchers reported that multicomponent hydrogel systems offer new prospects for diverse applications. The development of hydrogel hybrid systems containing nanoparticles (NPs) has gained much attention (Thakur et al. 2016; Makhado et al. 2020). The metal oxide nanoparticles act as fillers in the hydrogel matrix and enhance various properties such as thermal and mechanical properties, swelling, and adsorption capacity of the hydrogel nanocomposites (Deen and Chua 2015; Mittal and Ray, 2016, b; Makhado et al., 2019a, b, c). Among metal oxide nanoparticles, the magnetic iron oxide (Fe_3O_4) nanoparticles have attracted much research attention in various fields. In this context, Fe_3O_4 nanoparticles are classified as good adsorbents owing to their excellent low-toxicity, paramagnetic properties, and high surface-to-volume ratio (Cheng et al. 2016; Xu et al. 2014). The nanoparticles provide easy separation after adsorption by applying magnet (Xu et al. 2014). In this direction, there have been attempts to endow hydrogel-based nanocomposites with magnetic properties. Mittal et al. (2016) reported on the preparation of xanthan gum grafted poly(acrylic acid)-based Fe_3O_4 hydrogel nanocomposite in the adsorption of methyl violet. Their adsorbent exhibited an adsorption capacity of 642 mg/g (Mittal et al. 2016). In another study, Mittal et al. (2014) used XG-cl-p(AA-co-AAm)/Fe_3O_4 hydrogel nanocomposite for the removal of malachite green from aqueous solution. Mittal and Ray (2016, b) reported on the development of gum Ghatti–based iron oxide hydrogel nanocomposite for the remediation of MB-contaminated water, and obtained a maximum adsorption capacity of 671.14 mg/g. Nevertheless, the incorporation of Fe_3O_4 nanoparticles in the hydrogel matrix is limited due to high surface energy exhibited by Fe_3O_4 nanoparticles which may cause aggregation during preparation. To overcome this shortcoming, Fe_3O_4 nanoparticles are supported with clay to form a nanocomposite. The key role of clay is to control the morphology and distribution of Fe_3O_4 NPs in hydrogel hybrid systems.

Clay minerals have attracted considerable interest in material science research, particularly in the preparation of nanocomposite. In their pristine form, these materials are incompatible with most of the host systems. Therefore, the chemical modification of clay plays a vital role in nanocomposite and nanocomposite formation (Hato et al. 2011; Makhado and Ray 2015). Cloisite 30B (C30B) is functionalized with modified quaternary ammonium salts. Magdy et al. (2017) prepared a magnetic clay nanocomposite via the chemical co-precipitation method and evaluated the synthesized material as an adsorbent in the adsorption of the anionic C.I. Direct Red 23 dye. Due to the inherent weak structure of CMC, we hypothesize that the incorporation of Fe_3O_4-C30B in the CMC can act as a physical cross-linker to the polymer network to modify mechanical and thermal properties. In addition, the presence of magnetic nanoparticles in the hydrogel nanocomposite will play a crucial role during the separation process after adsorption.

In this study, we investigate the applicability and performance of CMC-cl-pAA hydrogel and its hydrogel nanocomposite synthesized via a free radical polymerization method in the adsorption of MB in aqueous solution. To the best of our knowledge, there is not much research done on the removal of MB from aqueous solution using magnetic CMC-

based hydrogel. Furthermore, this study aims to promote the use of low-cost CMC-based hydrogels in the removal of MB. The as-prepared materials were characterized by X-ray diffraction (XRD), Fourier transform infrared (FTIR), scanning electron microscopy (SEM), high-resolution transmission electron microscopy (HR-TEM), thermogravimetric analysis (TGA), and dynamic mechanical analysis (DMA). The applicability of CMC-cl-pAA hydrogel and CMC-cl-pAA/Fe_3O_4-C30B hydrogel nanocomposite as adsorbents in the removal of MB dye from the aqueous medium was systematically investigated. Through the adsorption kinetics, isotherms, and thermodynamics, the adsorption process of the adsorbents was examined.

Materials and methods

Materials

The biopolymer; sodium carboxymethyl cellulose (CMC); acrylic acid (AA, 99%) monomer; potassium persulfate (KPS) (≥ 98%; 248614) initiator; N,N′-methylene bisacrylamide (MBA, 99%) cross-linker; iron (III) chloride hexahydrate ($FeCl_3.6H_2O$); and iron (II) chloride tetrahydrate ($FeCl_2{\cdot}4H_2O$) were supplied by Sigma-Aldrich (South Africa). Acetone, sodium hydroxide (NaOH), ammonia solution (25%), and hydrochloric acid (HCl) were purchased from Merck (South Africa). Cloisite 30B (C30B) clay was supplied by Southern Clay Products (USA). All other reagents were of analytical grade and were used without further purification. Deionized (DI) water was used in the course of the experimental procedure. The stock solution of MB (1000 mg/L) was prepared by dissolving an appropriate amount of dye which was purchased from Merck (South Africa) in 1000 mL of DI water, and the stock solution was further diluted for batch experiments for adsorption studies.

Preparation of CMC-cl-pAA hydrogel

The method for the preparation of hydrogel was adopted from Thakur et al. (2016) with slight modifications. Briefly, a solution of CMC (0.15 g) in 100 mL DI water was prepared and mixed with calculated amounts of AA, KPS, and MBA to give a final volume of 40 mL. The reaction of graft copolymerization was initiated by exposing the mixture under a constant temperature of 70 °C for 3 h. The obtained CMC-cl-pAA hydrogel was allowed to cool at room temperature, cut into small pieces, and washed with acetone to remove unreacted reagents. The hydrogel was further washed with DI water, filtered, and vacuum-dried at 70 °C for 48 h and then milled to a fine powder. The optimum conditions of CMC-cl-pAA hydrogel were based on the swelling degree (*S*). The findings are displayed in Fig. S1 (a-c).

Preparation of magnetic C30B nanocomposite

Briefly, two separate solutions of $FeCl_3{\cdot}6H_2O$ (8.0 g) and $FeCl_2{\cdot}4H_2O$ (4.0 g) were prepared in 50 mL DI water. The two solutions were mixed and stirred thoroughly to obtain a homogenous mixture. To this mixture, 1.0 g of C30B in 50 mL DI water was added. The mixture was then stirred for 30 min at 50–60 °C using a magnetic stirrer. Ammonium solution was then added until a pH of 10 was obtained. The precipitated magnetic C30B was centrifuged for 10 min at 4000 rpm. The magnetic nanocomposite was washed numerous times with DI water, centrifuged, and dried at 70 °C for 24 h.

Preparation of CMC-cl-pAA/Fe_3O_4-C30B hydrogel nanocomposite

CMC (0.15 g) was dissolved in DI water. To this solution, calculated amounts of AA, KPS, and MBA were added, and the total volume was adjusted to 30 mL. To this mixture, 50 mg of Fe_3O_4-C30B was added slowly under constant stirring. The reaction of graft copolymerization was initiated by exposing the mixture under a constant temperature of 70 °C for 3 h. The obtained CMC-cl-pAA/Fe_3O_4-C30B hydrogel nanocomposite was allowed to cool at room temperature, cut into small pieces, and washed with acetone to remove unreacted reagents. The hydrogel nanocomposite was further washed with DI water, filtered, and vacuum-dried at 70 °C for 48 h and then milled to a fine powder. The schematic presentation for the preparation of the CMC-cl-pAA/Fe_3O_4-C30B hydrogel nanocomposite is given in Scheme 1. To optimize the adsorbent, the degree of swelling (*S*) studies were conducted and the results are presented in Fig. S2d.

Calculation of the degree of swelling

The degree of swelling (*S*) of the samples was investigated using DI water. In brief, 0.1 g of sample was immersed in 50 mL of distilled water at pH 7.0 for 24 h. The swollen sample was taken out of the water, blotted up with a filter paper, and weighed. The degree of swelling was calculated using the following:

$$S(\%) = \frac{W_s - W_d}{W_d} \times 100 \quad (1)$$

where *S* (%) is the degree of swelling of the hydrogel, W_s represents the mass of swollen hydrogel, and W_d represents the mass of the dry hydrogel.

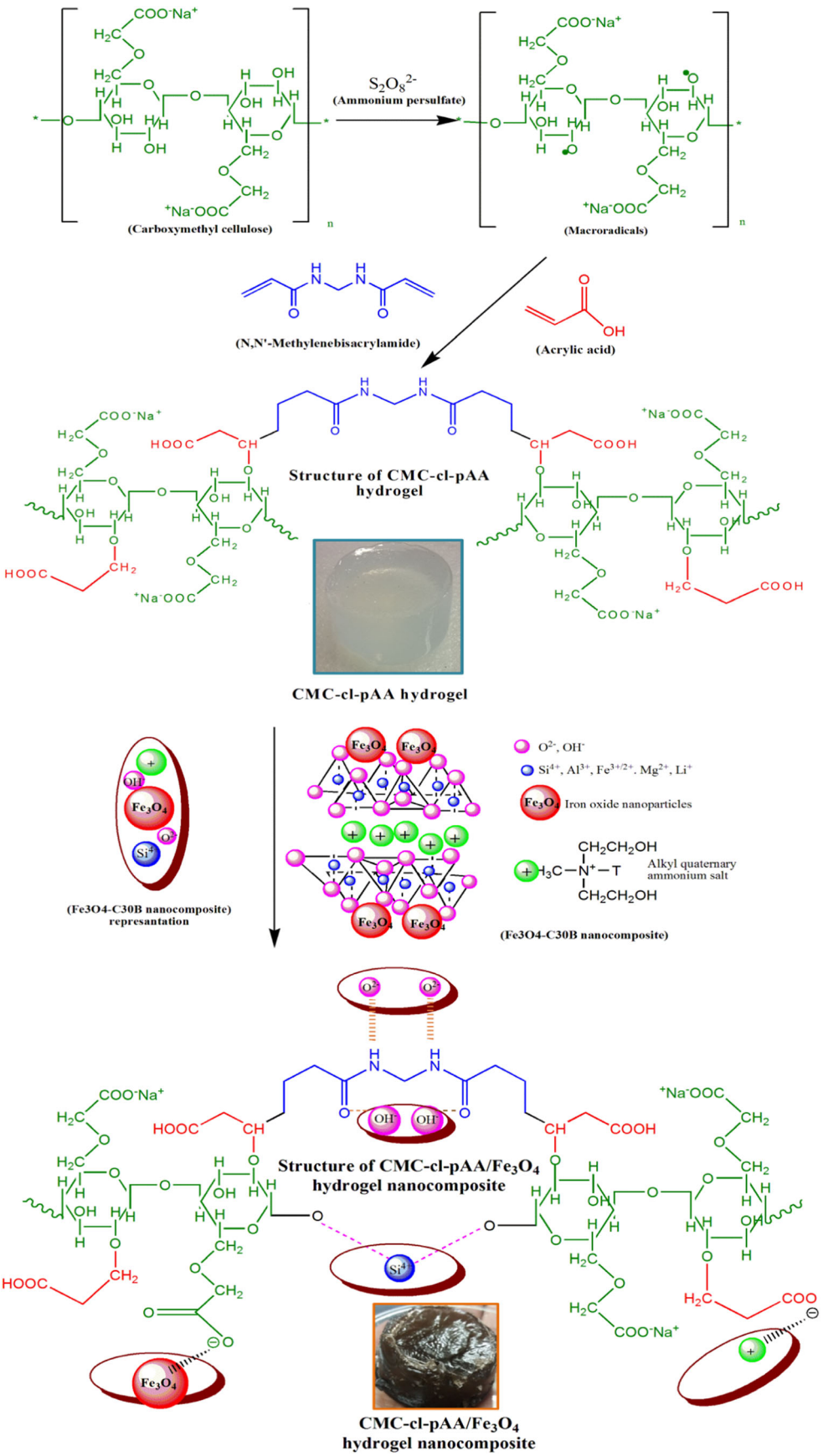

Scheme 1 Schematic presentation for the preparation of CMC-cl-pAA hydrogel and CMC-cl-pAA/Fe_3O_4-C30B hydrogel nanocomposite

Batch adsorption studies

The adsorption of MB dye was investigated in batch experiments. In brief, the optimum amount of adsorbent was added to a 100-mL PE plastic bottle containing 30 mL MB dye aqueous solution. The PE plastic bottles were agitated in the temperature-controlled oscillator set at 170 rpm. The effect of pH on the adsorption capacity ranged from 3.0 to 10.0. The solution pH was adjusted using (0.1 M) NaOH and (0.1 M) HCl solutions and recorded using Hanna (HI 9811-5) pH metre. The influence of adsorbent dose on the adsorption capacity was varied for 0.33 to 1.67 g/L. For the effect of contact time, the investigations were performed from 0 to 85 min. The influence of initial concentration was varied for 200 to 350 mg/L. After the adsorption process, the aliquots were filtered and the concentration was measured by UV-vis spectrophotometer (Cary 300) at λ_{max} of 662 nm. The adsorption percentage (%) and adsorption capacities (q_e) were determined using the following expressions:

$$\text{Adsorption}\ (\%) = \left(\frac{C_o - C_e}{C_o}\right) \times 100 \tag{2}$$

$$q_e = q_t = \left(\frac{C_o - C_e}{m}\right) V \tag{3}$$

where q_e and q_t represent the equilibrium capacity of MB on the adsorbent (mg/g) and the amount of MB adsorbed per unit mass of the adsorbent (mg/g) at a certain time t (min), respectively. C_o is the initial concentration of MB (mg/L), C_e is the equilibrium concentration of MB (mg/L), m is the mass of the adsorbent (g), and V is the volume of the MB dye solution (L).

Regeneration studies

Regeneration experiments were carried out by immersing the MB-loaded adsorbents into 50 mL of ethanol, and agitated at 170 rpm for 2 h. The collected absorbents were washed with DI water, dried at 50 °C, pulverized, and reused in the next cycle of adsorption. The dye adsorption/desorption runs were repeated four times.

Determination of point of zero charge

The point of zero charge (pH_{pzc}) is obtained from the difference between the initial and the final pH (ΔpH). To determine the pH_{pzc}, measured amounts of the hydrogel and the hydrogel nanocomposite were added in 30 mL of 0.1 M NaCl and the initial pH (pHi) was adjusted from 2 to 10 with 0.1 M HCl or 0.1 M NaOH solutions and agitated in a shaker (170 rpm, ambient temperature) for 48 h. The solution pH was recorded, and the pH_{pzc} was calculated as shown from the following Eq. (4):

$$\Delta pH = pH_{final} - pH_{initial} \tag{4}$$

Characterization techniques

The morphology and the elemental analysis of the prepared materials were investigated using the scanning electron microscopy (SEM) (JSM7500F, JEOL microscope, Tokyo, Japan). This was coupled with energy-dispersive X-ray spectrometer (EDS) operated at an acceleration voltage on 200 kV. Spectrum II spectrometer (Perkin-Elmer, Johannesburg, South Africa) Fourier transform infrared (FTIR) was employed to record FTIR spectra in the wavenumber range between 400 and 4500 cm^{-1} and resolution of 4 cm^{-1}. The X-ray diffraction (XRD) patterns were collected with a PAnalytical Xpert PRO-diffractometer (PAnalytical, Eindhoven, The Netherlands), employing Ni filtered CuKα radiation at a wavelength of 1.5406 Å. The thermal stability was performed by using a simultaneous thermal analyzer (STA) 6000 manufactured by Perkin-Elmer (Perkin-Elmer, Johannesburg, South Africa). The prepared samples were heated from 30 to 600 °C at a rate of 10 °C/min in a nitrogen atmosphere and the flow rate of 20 mL/min. To study the internal morphology of the samples, the high-resolution transmission electron microscopy (HR-TEM, JEOL JEM 2100 microscope, Tokyo, Japan) coupled with selected area electron diffraction (SAED) operated at 200 kV was employed. A dynamic mechanical analysis (DMA) was conducted on a single-cantilever bending mode using DMA 8000 (Perkin-Elmer, Johannesburg, South Africa) to study the mechanical stability of the hydrogels. The frequency dependence of the loss modulus and storage modulus were performed at a fixed temperature (30 °C). The strain amplitude was set at 0.05%, and the ramp rate was 5 °C/min in the frequency range of 0.01 to 100 Hz. An ultraviolet-visible spectrophotometer (UV-vis) was utilized to analyze the MB dye concentrations after adsorption.

Results and discussion

FTIR, XRD, and TGA analyses

The structural changes on CMC were confirmed by FTIR as revealed in Fig. 1a. The spectrum of CMC showed the presence of hydroxyl groups from 3000 to 3500 cm^{-1}, C–H stretching vibration at 2900 cm^{-1}, and vibrational bands related to carboxylates (COO^-) asymmetric (1652 cm^{-1}) and symmetric (1442 and 1392 cm^{-1}) stretch, which overlapped with the band of adsorbed water (Fekete et al. 2016; Wang et al.

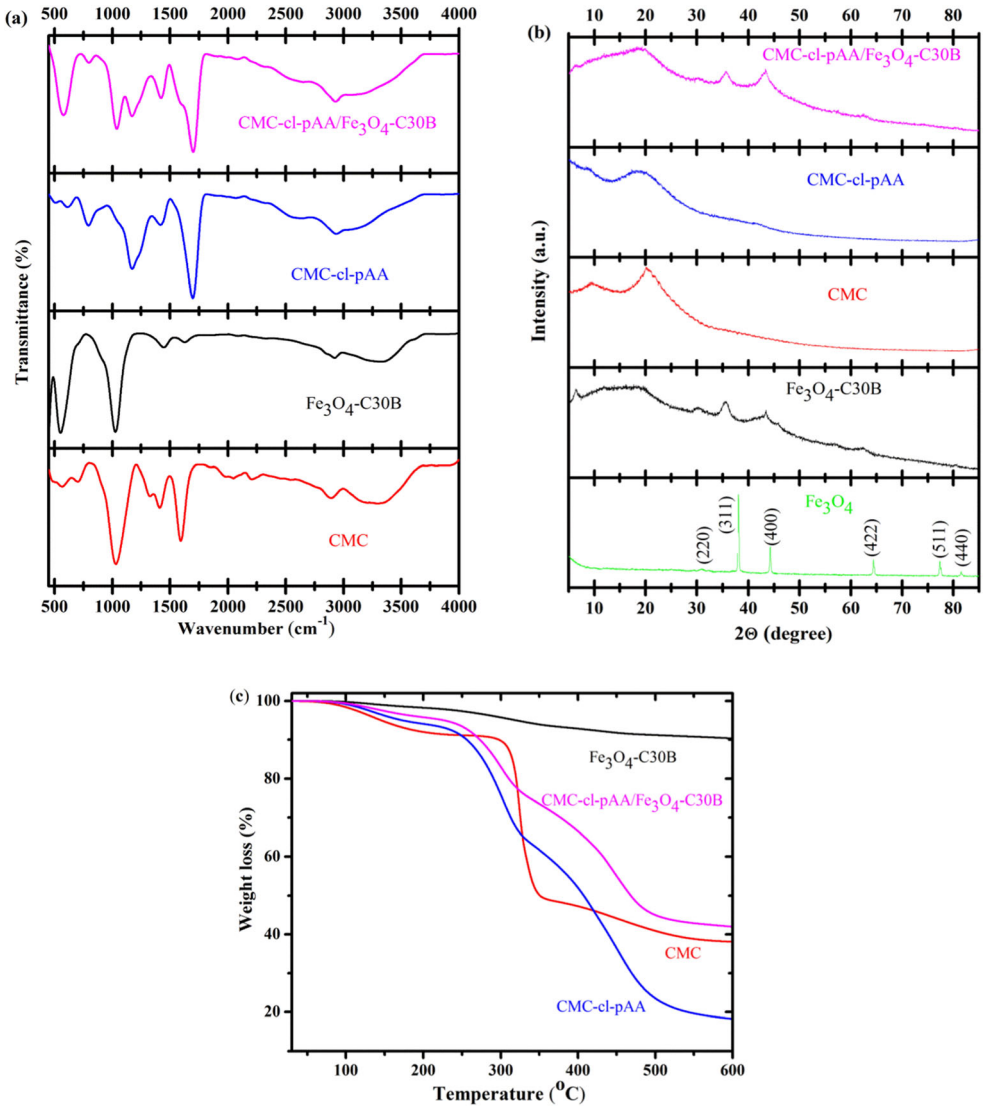

Fig. 1 **a** FTIR. **b** XRD spectra. **c** TGA of CMC, CMC-cl-pAA hydrogel, Fe_3O_4-C30B, and CMC-cl-pAA/Fe_3O_4-C30B hydrogel nanocomposite

2018). The band at 1040 cm^{-1} is assigned to the C–O–C stretching vibration. These observations are in good agreement with the results reported in the literature (Gao et al. 2018). After the grafting of AA onto CMC, there was a slight shift in the peaks and an increase in intensities. This could be attributed to the influence of the same functional groups emanating from the AA moieties. Furthermore, the characteristic absorption bands of CMC at about 392 cm^{-1} and 1040 cm^{-1} disappeared after grafting with AA, suggesting that the symmetric –OH in CMC molecules was chemically bonded to the AA during polymerization. Similar observations were as also reported by Salama (2015). Therefore, these observations confirm the successful synthesis of CMC-cl-pAA hydrogel. The FTIR spectrum of Fe_3O_4-C30B nanocomposite showed two major bands at 528 and 1080 cm^{-1} corresponding to the Fe–O band of the magnetite, and the Si–O–Si stretching of C30B, respectively (Fekete et al. 2016; Shen et al. 2018). These observations suggested the successful incorporation of magnetite nanoparticles onto the C30B surface. After the incorporation of Fe_3O_4-C30B nanocomposite onto CMC-cl-pAA hydrogel matrix, new peaks were observed on the CMC-cl-pAA/Fe_3O_4-C30B spectrum at approximately 1080 cm^{-1} and 528 cm^{-1}, which correspond to the Si–O–Si stretch of C30B clay and the Fe–O vibration of Fe_3O_4 (Magdy et al. 2017; Sitthichai et al. 2015). The appearance of these peaks confirms the successful preparation of CMC-cl-pAA/Fe_3O_4-C30B hydrogel nanocomposite.

The structure and crystalline features of Fe_3O_4 nanoparticles and Fe_3O_4-C30B nanocomposite were assessed by the XRD analysis (Fig. 1b). The diffraction pattern of Fe_3O_4 nanoparticles exhibited pearls at 2θ = 32.2° (220), 38.0° (311), 44.4° (400), 64.7° (422), 78.1° (511), and 83.5° (440) corresponding to the characteristic diffractions of Fe_3O_4 nanoparticles (Shen et al. 2018; Loh et al. 2008). These results

indicate high crystalline phase purity of the nanoparticles. Fe_3O_4-C30B nanocomposite showed two peaks at 2θ = 37.0° and 44.1° emanating from Fe_3O_4 nanoparticles. Upon the nanocomposite formation, the patterns shifted to lower 2θ values as compared to Fe_3O_4 nanoparticles, and other peaks from Fe_3O_4 nanoparticles disappeared. Diffractogram of CMC showed two pronounced broad peaks observed at 2θ = 9.0° and 2θ = 21.8°, suggesting low crystallinity (Ninan et al. 2013). After the graft copolymerization of AA onto CMC, the peaks emanating from CMC emerged and formed a broad diffraction peak at 2θ = 21.8°, demonstrating the glassy amorphous nature of the hydrogel composite (Salama, 2015). According to Shen et al. (2018), the disruption of the ordered arrangement of CMC indicated that copolymerization had taken place. The CMC-cl-pAA/Fe_3O_4-C30B hydrogel nanocomposite diffractogram showed amorphous broad peak at 2θ = 18.5° associated with the CMC. Furthermore, new characteristic peaks were observed at 2θ = 38.0° and 44.4° corresponding to 311 and 400 of planes, respectively. This result confirms the presence of Fe_3O_4-C30B nanocomposite in the hydrogel matrix, which agrees very well with the FTIR results (Fig. 1a).

The TGA was used to determine the precise weight ratio of each component in a sample, and the thermal stability of the hydrogel and its nanocomposite. The TGA thermograms of CMC, Fe_3O_4-C30B nanocomposite, CMC-cl-pAA hydrogel, and CMC-cl-pAA/Fe_3O_4-C30B hydrogel nanocomposite are depicted in Fig. 1c. It can be seen that the CMC exhibits two thermal degradation steps throughout the experimental temperature range. These two steps appear at about 100 and 315 °C, and are normally associated with the evaporation of water at about 10 wt% loss and polysaccharide backbone decomposition at about 45 wt%, respectively (Shen et al. 2018). The CMC-cl-pAA hydrogel shows two degradation stages at 100–250 °C due to the loss of moisture in the structure followed by the second degradation in the range 330–500 °C owing to the CMC polymer chains (Shen et al. 2018; Mishra et al. 2011). The degradation of CMC-cl-pAA/Fe_3O_4-C30B hydrogel nanocomposite also took place in two steps. The initial degradation step shows weight loss from 112 to 317 °C, which could be attributed to the loss of moisture and solvents (Soliman et al. 2016). The second degradation step could be attributed to the disruption of the cross-links in the polymer structure, and the decomposition of the CMC-cl-pAA/Fe_3O_4-C30B hydrogel nanocomposite (Shen et al. 2018; Loh et al. 2008; Makhado et al., 2019a, b, c). The lower rate of mass loss with increasing temperature may be due to the internal change in this material that is not accompanied by a mass loss at elevated temperature. The slower, less steep degradation step in the case of the hydrogel nanocomposite suggested higher thermal stability due to the stabilizing effect of Fe_3O_4-C30B nanocomposite. TGA curves demonstrated that the incorporation of Fe_3O_4-C30B nanocomposite in the hydrogel matrix enhanced the thermal stability of hydrogel. This behaviour could be due to the multifunctional cross-linking between the CMC-cl-pAA hydrogel and Fe_3O_4-C30B nanocomposite.

Morphological characteristics

The morphology of the CMC, Fe_3O_4-C30B nanocomposites, CMC-cl-pAA hydrogel, and CMC-cl-pAA/Fe_3O_4-C30B hydrogel nanocomposite is presented in Fig. 2. SEM images of the synthesized samples are given in Fig. 2a–d and EDS result in Fig. 2e. As seen in Fig. 2a, the surface morphology of the CMC image shows the coarse structure, indicating an amorphous nature of the material. Upon grafting of AA onto CMC (Fig. 2b), well-defined CMC interconnections with irregular shape was observed (Salama 2018). The image in Fig. 2c shows tiny spherical magnetite nanoparticles on the surface of the organoclay sheets (Abreu et al. 2015). In Fig. 2d, a rough irregular surface morphology with well-defined interconnections was noticed in the case of the CMC-cl-pAA/Fe_3O_4-C30B hydrogel nanocomposite. This is due to the presence of C30B and Fe_3O_4 nanoparticles in the hydrogel matrix (Bao et al. 2011; Abreu et al. 2015). Furthermore, the existence of Fe_3O_4-C30B nanocomposite in the hydrogel was confirmed by the EDS analysis (Fig. 2e), which revealed the presence of O, Fe, Si, Al, K, and S as the elemental compositions due to Fe_3O_4 nanoparticles and C30B in the hydrogel nanocomposite.

Figure 3a and b show the TEM images of Fe_3O_4-C30B and CMC-cl-pAA/Fe_3O_4-C30B hydrogel nanocomposite. The figures show that the agglomerated magnetite nanoparticles are homogeneously dispersed on the surface of the C30B sheets. The HR-TEM of the magnetite nanoparticles (Fig. 3c) showed that lattice fringes could be observed, and revealed a crystalline structure with the characteristic d-spacing of 0.2505 nm. This d-spacing of 0.2505 nm correspond to the (311) planes of magnetite (Chin et al. 2008). This result is in good agreement with the XRD results (Fig. 1b). The corresponding selected area electron diffraction (SAED) pattern was employed to further investigate the crystallinity of the CMC-cl-pAA/Fe_3O_4-C30B hydrogel nanocomposite (Fig. 3d). From the SAED pattern, a white dash line circle, which is a characteristic of the crystal structure, is observed (Acp et al. 2015). Dotted concentric rings were observed. These rings occur as a result of the diffraction of particles of different orientations of the cubic Fe_3O_4 nanoparticles (Sitthichai et al. 2015). Nevertheless, the scattered white light from the nanoparticles is not noticeable as compared with the CMC-coated Fe_3O_4 nanoparticles reported by Sitthichai et al. (2015). This observation could be due to the CMC-cl-pAA hydrogel and C30B loading. From these observations, we can infer that the hydrogel nanocomposite possessed both crystalline and amorphous properties as also observed from XRD results.

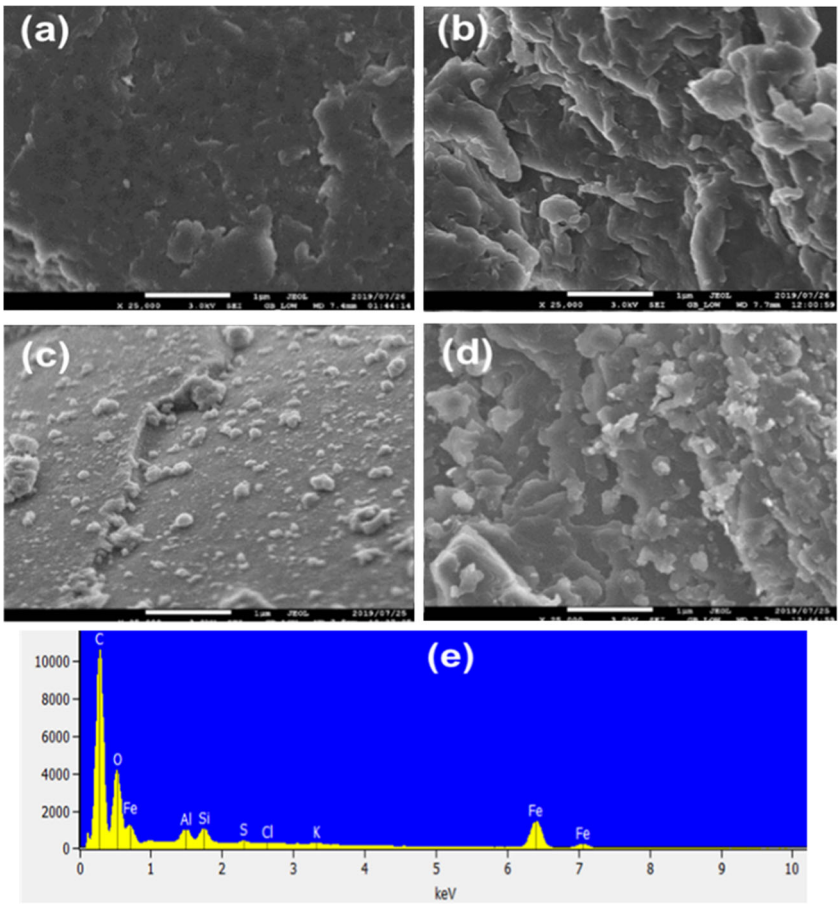

Fig. 2 SEM images of **a** resolution 25× of CMC, **b** CMC-cl-pAA hydrogel, **c** Fe_3O_4-C30B, **d** CMC-cl-pAA/Fe_3O_4-C30B hydrogel nanocomposite, and **e** EDS analysis of CMC-cl-pAA/Fe_3O_4-C30B hydrogel nanocomposite

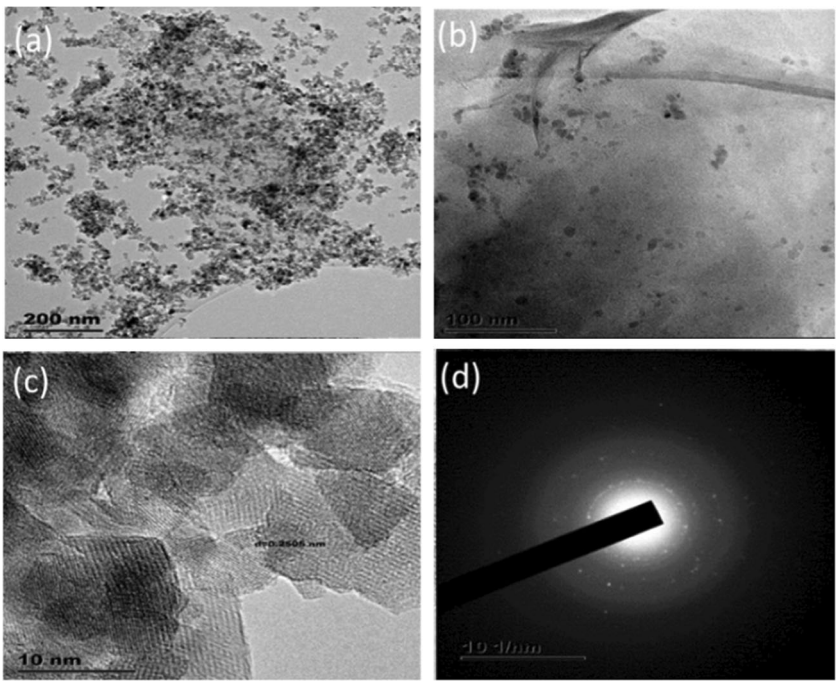

Fig. 3 TEM images of **a** Fe_3O_4-C30B, **b** CMC-cl-pAA/Fe_3O_4-C30B hydrogel nanocomposite, **c** HR-TEM image of Fe_3O_4-C30B, and **d** SAED pattern of CMC-cl-pAA/Fe_3O_4-C30B hydrogel nanocomposite

Dynamic mechanical analysis

The DMA was used to measure the response of the CMC-cl-pAA hydrogel and CMC-cl-pAA/Fe_3O_4-C30B hydrogel nanocomposite to an oscillatory deformation in tension-torsion mode as a function of frequency. Figure 4a shows the storage modulus response to the frequency of CMC-cl-pAA hydrogel and CMC-cl-pAA/Fe_3O_4-C30B hydrogel nanocomposite. Both hydrogel and its nanocomposite showed a similar trend, whereby the storage modulus of both samples increased with increasing frequency until a linear region (plateau) was reached. This observation suggested stable network structures with no deformation as the oscillation frequency increased (Makhado et al. 2020). However, it was noticeable that the CMC-cl-pAA/Fe_3O_4-C30B hydrogel nanocomposite exhibited higher storage modulus than its counterpart. This result suggests that the polymeric hydrogel had weak cross-linking density, while the CMC-cl-pAA/Fe_3O_4-C30B hydrogel nanocomposite was characterized by more solid-like behaviour. A more solid-like behaviour in the case of the CMC-cl-pAA/Fe_3O_4-C30B hydrogel nanocomposite indicates that this material can store deformation energy better than the bare hydrogel (Khedmat et al., 2013). These findings are in agreement with the results reported by Peng et al. (2016). Moreover, an increase in the storage modulus is due to the high cross-linking density, which restricts the movement of the polymer segment (Yue et al. 2019) owing to the incorporation of inorganic components within the hydrogel polymer, resulting in enhanced mechanical properties (Li et al. 2019). Furthermore, an improvement in the mechanical stability of the magnetic hydrogel nanocomposite may be due to the strong hydrogen bonding between the COO^- of CMC and the –OH groups of C30B clay (Mahdavinia et al. 2017; Wittenberg et al. 2018). Again, the addition of C30B clay in the hydrogel has been reported to act as a multifunctional cross-linker, increasing the cross-linking density of the gel, which limits the hydrogel volume expansion and subsequently leading to an improved gel structure and stability (Mahdavinia et al. 2017; Fekete et al. 2016). The metal cations such as the Fe^{3+} of Fe_3O_4 can form coordination bonds with the negatively charged hydrogel polymer chains to increase the cross-linking density (Zhu et al. 2017). These coordination bonds can act as reversible sacrificial bonds that break to dissipate any applied energy, thus improving the storage modulus (Zhu et al. 2017). The homogeneous dispersion of nanofiller in the polymer network could improve the storage modulus of the resultant polymer nanocomposite (Hato et al. 2008).

Figure 4b displays the viscous behaviour of CMC-cl-pAA hydrogel and CMC-cl-pAA/Fe_3O_4-C30B hydrogel nanocomposite as a function of frequency. The loss modulus of CMC-cl-pAA/Fe_3O_4-C30B hydrogel nanocomposite was slightly higher than that of CMC-cl-pAA hydrogel in the frequency range of 0.01 to 100 Hz. As seen in Fig. 4a, the storage modulus showed higher values compared with the loss modulus (Fig. 4b), which suggests that the hydrogel nanocomposite has higher capacity to store the energy.

Adsorption studies

Effect of solution pH on the adsorption of MB dye

The pH of the solution affects the adsorption process to a greater extent and is the most vital parameter for the adsorption of water pollutants (Maponya et al. 2020). The pH governs the interaction between adsorbate molecules and the surface of the adsorbent during the adsorption process (Thakur et al. 2016; Makhado et al. 2018a, b; Hu et al. 2018). The effect of solution pH in the removal of MB using CMC-cl-pAA hydrogel and CMC-cl-pAA/Fe_3O_4-C30B hydrogel nanocomposite was studied by varying the initial solution pH from 3.0 to 10.0 at 25 °C. The results are depicted in Fig. 5a. It is known that CMC and AA monomer contain hydrophilic carboxylic groups (COO^-) on their surfaces

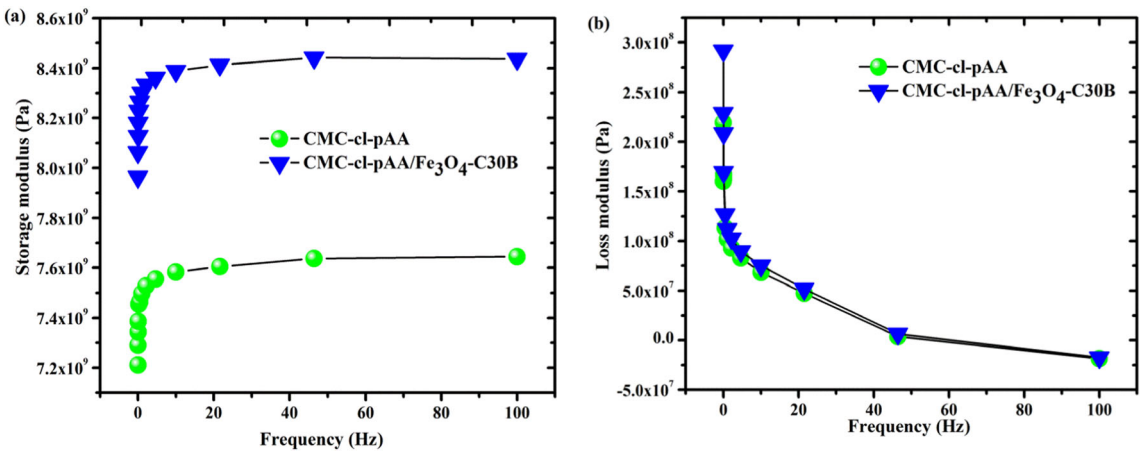

Fig. 4 **a** Storage modulus and **b** loss modulus of CMC-cl-pAA hydrogel and CMC-cl-pAA/Fe_3O_4-C30B hydrogel nanocomposite

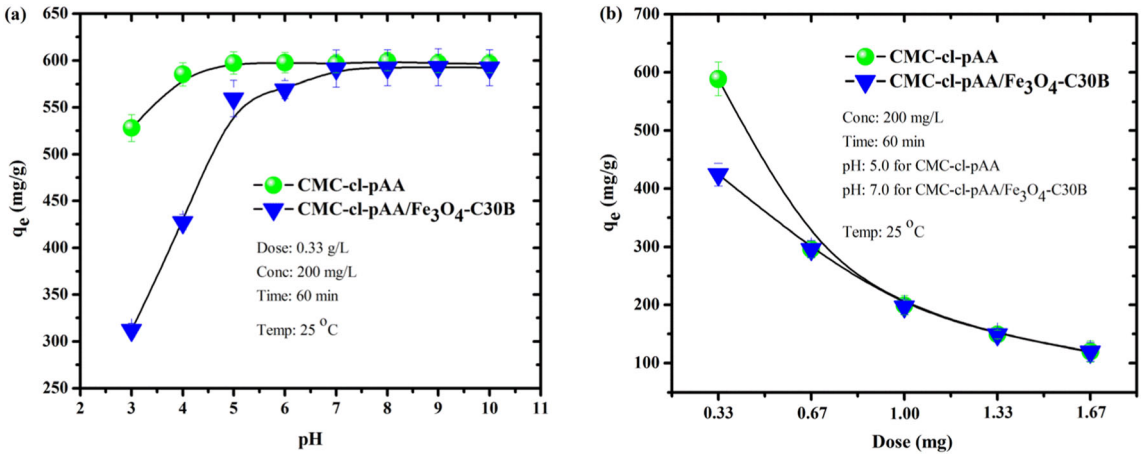

Fig. 5 **a** Effect of solution pH and **b** adsorbent dose on the removal of MB by CMC-cl-pAA hydrogel and CMC-cl-pAA/Fe_3O_4-C30B hydrogel nanocomposite

(Makhado et al. 2018a). At a lower pH, the active sites are protonated, resulting in the repulsion between the positive adsorbent and the cationic MB dye molecules (Makhado et al. 2018b). When the pH of the solution pH was increased from 3.0 to 10.0, the adsorption capacities of CMC-cl-pAA hydrogel and CMC-cl-pAA/Fe_3O_4-C30B hydrogel nanocomposite increased from 528 to 597 mg/g and 312 to 592 mg/g, respectively. The adsorption equilibrium was obtained at pH 5.0 for bare hydrogel and pH 7.0 for the CMC-cl-pAA/Fe_3O_4-C30B hydrogel nanocomposite. Thereafter, there was no noticeable increase in the pH of the MB solution at the end of the adsorption process. At higher pH, the active sites become negatively charged, which encourages electrostatic interaction between the adsorbate (COO^-) and the cationic MB dye molecules. Thus, the adsorption capacity was increased for both CMC-cl-pAA hydrogel and CMC-cl-pAA/Fe_3O_4-C30B hydrogel nanocomposite.

To study the surface charge of CMC-cl-pAA hydrogel and CMC-cl-pAA/Fe_3O_4-C30B hydrogel nanocomposite, the pH_{pzc} was performed and the plot of ΔpH as a function of $pH_{initial}$ is depicted in the Supplementary Information (Fig. S2a,b). The pH_{pzc} of CMC-cl-pAA hydrogel and CMC-cl-pAA/Fe_3O_4-C30B hydrogel nanocomposite are 3.13 and 3.63, respectively. At pH > pH_{pzc}, the surface of adsorbents had a net positive charge, while at pH < pH_{pzc}, the surface had a net negative charge. Both adsorbents showed a similar trend throughout the studied pH range. However, CMC-cl-pAA/Fe_3O_4-C30B hydrogel nanocomposite displayed a slightly higher pH_{pzc} than CMC-cl-pAA hydrogel. These results confirm that the incorporation of Fe_3O_4-C30B nanocomposite on the CMC-cl-pAA hydrogel network altered the surface change. These findings suggest that the change in the pH value during the adsorption process can induce changes in the adsorption pathways. The effect of pH on the adsorption was explained by strong electrostatic attraction between synthesized adsorbents and MB molecules. Makhado et al. (2018a, b) observed similar trends in the case of xanthan gum-cl-poly acrylic acid/oxidized MWCNTs (XG-cl-pAA/o-MWCNTs) hydrogel nanocomposite.

Effect of adsorbent dose

The effect of the adsorbent dose was investigated using 0.33 to 1.67 g/L of the hydrogel and hydrogel nanocomposite. The results are presented in Fig. 5b. It could be seen that the adsorption capacity of both CMC-cl-pAA hydrogel and CMC-cl-pAA/Fe_3O_4-C30B hydrogel nanocomposite decreased with increasing adsorbent dose. Hu et al. (2018) reported that at a lower adsorbent dose, the active sites fully take part in adsorbing MB, resulting in a higher adsorption capacity. However, at a high dose, it is noticeable that the equilibrium is readily reached owing to the presence of osmotic pressure despite the abundance of active sites. These results could be due to the agglomeration of the active sites on the adsorbent surface and the heightened diffusion path length responsible for the reduction in the adsorption capacity (Makhado et al. 2018a). However, it was clear from the figure that the adsorption capacity of the CMC-cl-pAA hydrogel was higher compared with the CMC-cl-pAA/Fe_3O_4-C30B hydrogel nanocomposite. This could be attributed to the highly cross-linked structure of the polymer caused by incorporating nanofillers (Soppiranth and Aminabhavi, 2002).

Adsorption kinetic studies

Adsorption kinetics rate equations are important in determining the rate of adsorbing MB. Figure 6a shows the dependence of adsorption on the contact time. It could be seen that with increasing contact time, the adsorption capacity of both CMC-cl-pAA hydrogel and CMC-cl-pAA/Fe_3O_4-C30B hydrogel

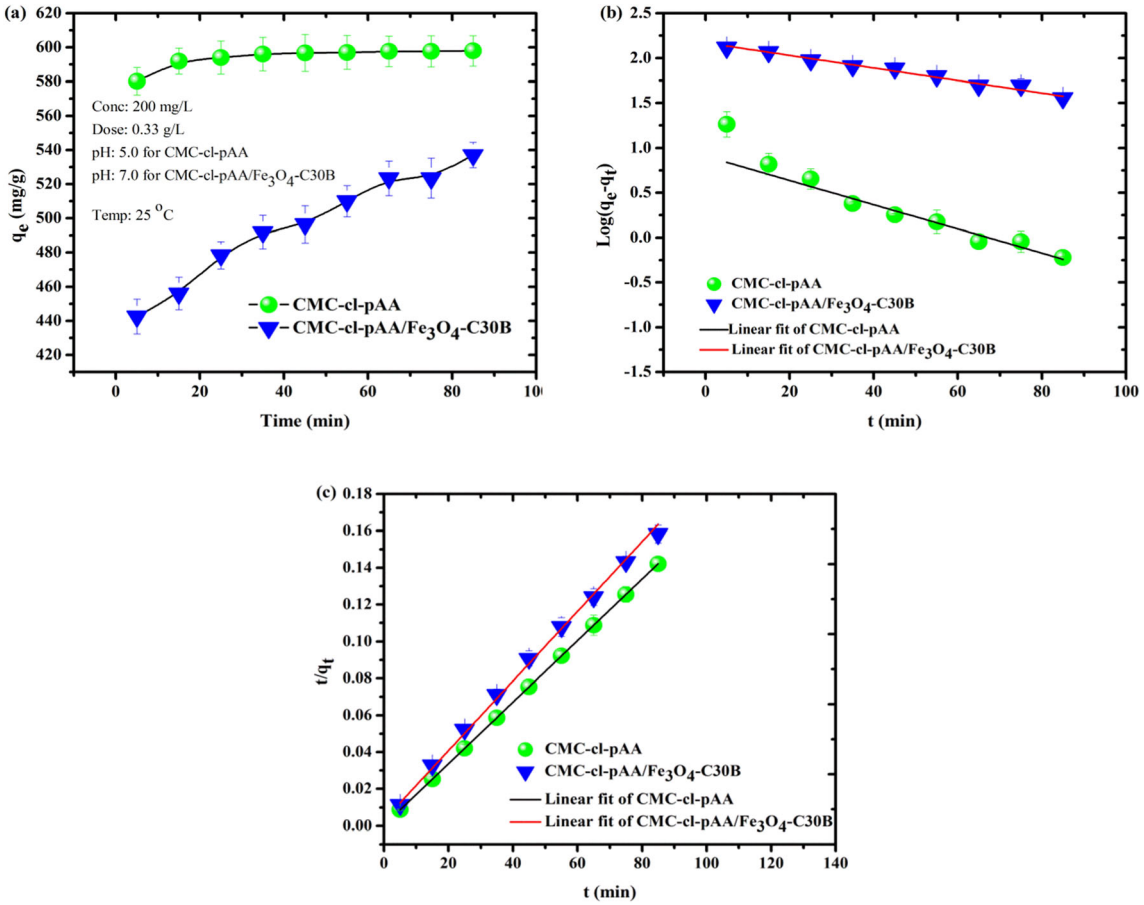

Fig. 6 **a** Effect of contact time. **b** Pseudo-first-order and **c** pseudo-second-order kinetics models for CMC-cl-pAA hydrogel and CMC-cl-pAA/ Fe_3O_4-C30B hydrogel nanocomposite

nanocomposite increased. This could be due to enough time given for the anionic adsorbent to interact with the cationic MB. Furthermore, these results showed that the adsorption equilibrium was reached after 25 min in the case of CMC-cl-pAA hydrogel. This implies that the adsorption of MB by CMC-cl-pAA hydrogel was faster than that of the CMC-cl-pAA/Fe_3O_4-C30B hydrogel nanocomposite. These experimental data were used to analyze the pseudo-first-order and pseudo-second-order.

Details of pseudo-first-order and pseudo-second-order kinetics models are given in the Supporting Information. The plots of In ($q_e - q_t$) against t and t/q_t versus t are depicted in Fig. 6b, c. The fitting parameters of pseudo-first-order and pseudo-second-order models are given in Table S1. Based on the correlation coefficient (R^2), the pseudo-second-order was higher (0.999) than that of the pseudo-first-order for both adsorbents. Moreover, the calculated RMSE value favoured the pseudo-second-order model as a probable kinetic model. This implies that the surface adsorption was the rate-limiting step and was governed by chemisorption interactions.

Adsorption isotherm studies

The effect of initial MB concentration on the adsorption capacity was evaluated and the results are presented in Fig. 7a. It could be noticed that the adsorption capacity of CMC-cl-pAA hydrogel and CMC-cl-pAA/Fe_3O_4-C30B hydrogel nanocomposite augmented from 499.5 to 1033.5 mg/g and 499.5 to 988.5 mg/g when the initial concentration was increased from 200 to 350 mg/L, respectively. The increase in the adsorption capacity with increasing initial concentration demonstrates that mass gradient functions as the driving force of the adsorption process (Soppiranth and Aminabhavi, 2002; Mahdavinia et al. 2017). In addition, an increase in the MB concentration in bulk solution at fixed CMC-cl-pAA hydrogel and CMC-cl-pAA/Fe_3O_4-C30B hydrogel nanocomposite dosage raises the mass transfer process. The above experimental data were modelled with Langmuir, Freundlich, and Temkin adsorption isotherm models.

The adsorption isotherm models are essential for estimating the nature of the adsorbate-adsorbent interactions and the distribution of the adsorbates between adsorbents and aqueous

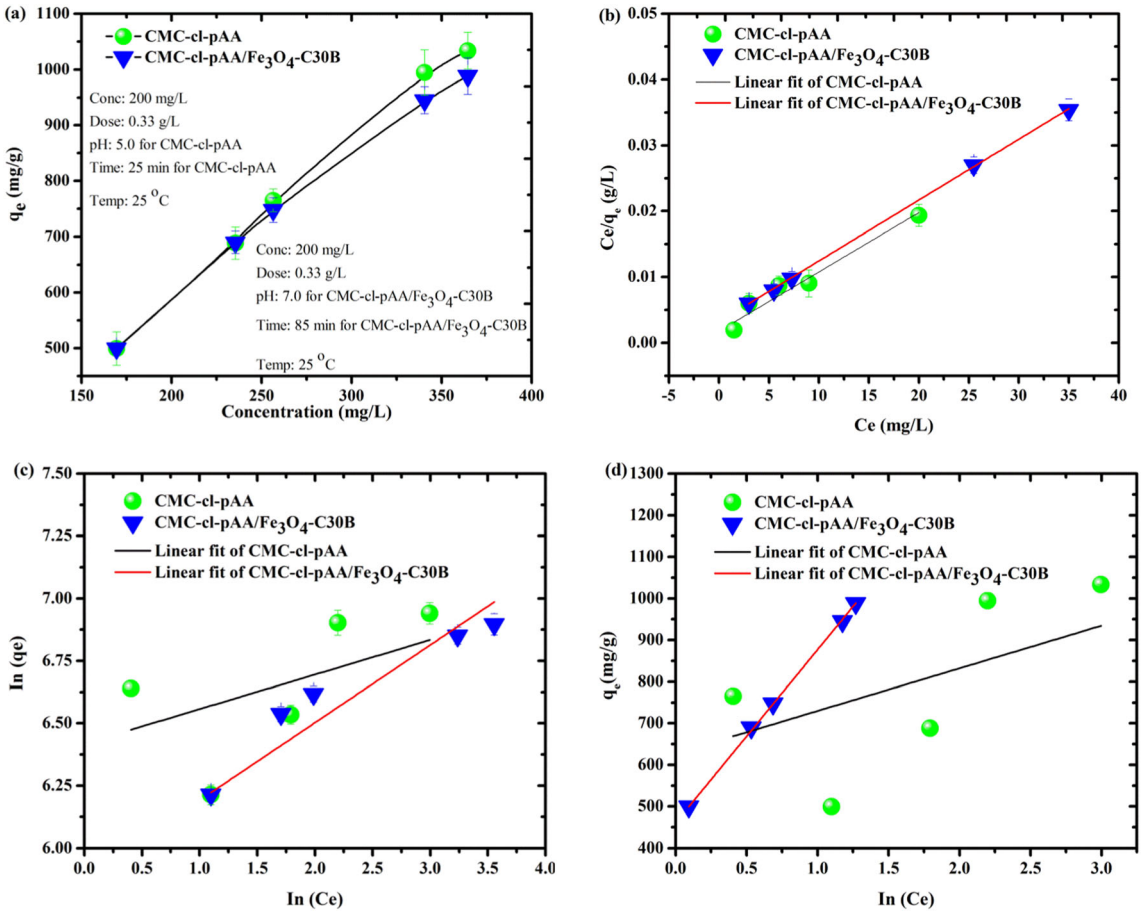

Fig. 7 **a** Effect of concentration, **b** Langmuir, **c** Freundlich, and **d** Temkin isotherm models for CMC-cl-pAA hydrogel and CMC-cl-pAA/Fe_3O_4-C30B hydrogel nanocomposite

phases in the adsorption process. Details of the mentioned isotherm models are discussed in the supporting information. The results are shown in Fig. 7b–d and Table 1. The applicability of these models was compared with the highest R^2 and lower RMSE values. According to the adsorption isotherm results, the Langmuir isotherm model better described

Table 1 Adsorption isotherm model results for CMC-cl-pAA hydrogel and CMC-cl-pAA/Fe_3O_4-C30B hydrogel nanocomposite

Isotherm models	Isotherm constants	CMC-cl-pAA hydrogel	CMC-cl-pAA/Fe_3O_4-C30B hydrogel nanocomposite
Langmuir	q_m (mg/g)	1109.55	1081.60
	b	0.509	0.289
	R_L	0.115–0.005	0.020–0.0009
	R^2	0.977	0.999
	RMSE	6.84×10^{-4}	1.45×10^{-5}
Freundlich	n	7.228	3.217
	K_F	613.1	358.1
	R^2	0.637	0.974
	RMSE	0.127	2.901
Temkin	A_T (L/g)	461.2	3.026
	b_T (kJ mol^{-1})	20.66	5.955
	β (J mol^{-1})	120.3	416.5
	R^2	0.558	0.999
	RMSE	116.3	0.188

the MB dye adsorption by CMC-cl-pAA hydrogel. The Langmuir isotherm model had the highest R^2 value of 0.977 and the lowest RMSE value of 6.84×10^{-4}. The R^2 values decreased in the order: Langmuir > Freundlich > Temkin. This result demonstrated the monolayer adsorption dominant adsorption process. In the case of CMC-cl-pAA/Fe_3O_4-C30B hydrogel nanocomposite, the Langmuir and Temkin isotherms were the best fit for describing the adsorption process. Both Langmuir and Temkin isotherm exhibited the highest R^2 value (0.999). However, from RMSE values, both Langmuir and Temkin isotherm models are considered excellent owing to their RMSE < 0.1 and RMSE between 0.1 and 0.2, respectively. The maximum adsorption capacity was found to be 1109.55 mg/g (CMC-cl-pAA hydrogel) and 1081.60 mg/g for CMC-cl-pAA/Fe_3O_4-C30B hydrogel nanocomposite. These results substantiate the monolayer adsorption of MB onto CMC-cl-pAA/Fe_3O_4-C30B hydrogel nanocomposite.

Since Langmuir and Temkin isotherm models were favoured, these results substantiate that the adsorption of MB on the CMC-cl-pAA/Fe_3O_4-C30B hydrogel nanocomposite occurred in a monolayer coverage. This implied that the active sites attracted the MB molecules with the same amount of energy such that a single layer of homogeneous adsorption was obtained. The R_L values were found to be in the range of 0.115–0.005 and 0.020–0.0009 for CMC-cl-pAA hydrogel and CMC-cl-pAA/Fe_3O_4-C30B hydrogel nanocomposite, respectively. This result indicates that the adsorption of MB was favourable ($0 < R_L < 1$). The results demonstrate that CMC-cl-pAA hydrogel is a more efficient adsorbent in the removal of MB dye from aqueous solution in comparison to the CMC-cl-pAA/Fe_3O_4-C30B hydrogel nanocomposite. Temkin results revealed that there may be physical and chemical interactions between adsorbate and adsorbent.

The maximum adsorption capacity obtained in the present study was compared with adsorption capacities of other adsorbents reported in the literature in the removal of MB. The results are shown in Table 2 (Dai et al. 2018; Benhalima et al. 2017; Liu et al. 2015; Hosseinzadeh and Khoshnood 2016; Capanema et al. 2018; Lin et al. 2017; Su et al. 2018; Atta et al. 2013; Sun et al. 2015). The synthesized CMC-cl-pAA hydrogel and CMC-cl-pAA/Fe_3O_4-C30B hydrogel nanocomposite possessed the maximum adsorption capacity values of 1109.55 and 1081.60 mg/g, respectively. It is noticeable that maximum adsorption capacities obtained in this study are greater than most of the reported values in the literature.

Although CMC-cl-pAA/Fe_3O_4-C30B hydrogel nanocomposite exhibited comparatively lower adsorption capacity (1081.60 mg/g) than that of CMC-cl-pAA hydrogel (1109.55 mg/g), this hydrogel nanocomposite showed enhanced properties such as mechanical and thermal stability, which are essentials for the practical use of adsorbents. Furthermore, the presence of Fe_3O_4 nanoparticles in the hydrogel matrix provides the adsorbent with paramagnetic properties for easy separation after adsorption by applying magnet (Fig. S3).

Adsorption thermodynamics and regeneration studies

To explore the adsorption thermodynamics during the MB adsorption by the hydrogel and its nanocomposite, experiments were performed at different temperatures ranging from 25 to 45 °C. The thermodynamic parameters were applied to

Table 2 Comparison of the synthesized CMC-cl-pAA hydrogel and CMC-cl-pAA/Fe_3O_4-C30B hydrogel nanocomposite with other adsorbents for MB removal

Adsorbents	Maximum adsorption capacity (mg/g)	References
PVA/CMC hydrogel*	83.33	Dai et al. 2018
CMC-based hydrogel beads	82.00	Benhalima et al. 2017
Regenerated CMC-based hydrogel beads	350.00	Benhalima et al. 2017
Hydroxypropylcellulose (HPC)/graphene oxide	118.48	Liu et al. 2015
Poly(AA-co-AMPS)/MMT*	192.31	Hosseinzadeh and Khoshnood 2016
CMC-based hydrogels	5–25.00	Capanema et al. 2018
MCA–E/CMC microspheres*	998.20	Lin et al. 2017
Magnetic carboxyl functional nanoporous polymer	57.74	Su et al. 2018
Fe_3O_4/p(Am-co-Na Ac)*	635.60	Atta et al. 2013
Xylan/pAA/Fe_3O_4	438.60	Sun et al. 2015
CMC-cl-pAA hydrogel	1109.55	Present study
CMC-cl-pAA/Fe_3O_4-C30B hydrogel nanocomposite	1081.60	Present study

**PVA*, polyvinyl alcohol; *MCA-E/CMC*, monochloroacetic acid-epichlorohydrin carboxymethyl cellulose; *p(Am-co-Na Ac)*, poly(acrylamide-co-sodium acrylate); *poly(AA-co-AMPS)/MMT*, poly(acrylic acid-co-acrylamido-2-methyl-1-propanesulfonic acid)/montmorillonite

evaluate the orientation and feasibility of the MB dye adsorption by CMC-cl-pAA hydrogel and CMC-cl-pAA/Fe_3O_4-C30B hydrogel nanocomposite. Thermodynamics parameters such as the change in the Gibbs free energy ($\Delta G°$, kJ/mol), enthalpy ($\Delta H°$, kJ/mol), and entropy, $\Delta S°$ (J/mol K) were determined from the plot of ln (q_e/C_e) depicted in Fig. 8a with the help of Eqs. S10 and S11. The results are given in Table S2. The obtained values of ΔH (− 306.9 kJ/mol) and $\Delta S°$ (− 0.365 kJ/mol/K) for CMC-cl-pAA hydrogel indicate an exothermic reaction with less disorder (Melo et al. 2018; Song et al. 2016). In contrast, $\Delta H°$ (887.9 kJ/mol) and $\Delta S°$ (3.396 kJ/mol/K) for CMC-cl-pAA/Fe_3O_4-C30B hydrogel nanocomposite were positive, suggesting an endothermic reaction with more disorder and randomness at the solid or solution interface during the adsorption process (Melo et al. 2018). The negative change in $\Delta G°$ values for both bare hydrogel and hydrogel nanocomposite implies the feasibility and spontaneous nature of the adsorption process (Dogan et al. 2009). The spontaneous endothermic reaction for CMC-cl-pAA/Fe_3O_4-C30B hydrogel nanocomposite is possible when the entropy increases by more than the change in enthalpy with increasing temperature (Song et al. 2016; Mahmoodi et al. 2012). These observations confirm the increase in the adsorption capacity as temperature increases. The adsorption of MB by the hydrogel and the hydrogel nanocomposite was dominated by chemisorption since $\Delta G°$ was between − 80 and − 400 kJ/mol (Mahmoodi et al. 2012). These results are in good accord with the pseudo-second-order rate law discussed in the previous section.

Practical applicability, stability, and reusability play an important role in the adsorption process. Four cycles of adsorption-desorption were carried out to investigate the regeneration of synthesized adsorbents (Fig. 8b). The results revealed that both CMC-cl-pAA hydrogel and CMC-cl-pAA/Fe_3O_4-C30B hydrogel nanocomposite maintained high adsorption percentage even after four successive cycles under the same conditions. Nonetheless, CMC-cl-pAA/Fe_3O_4-C30B hydrogel nanocomposite showed that there was no significant reduction in the adsorption percentage, which implied that CMC-cl-pAA/Fe_3O_4-C30B hydrogel nanocomposite was more stable for the adsorption of MB in an aqueous solution than CMC-cl-pAA hydrogel. Furthermore, as seen in Fig. S3,

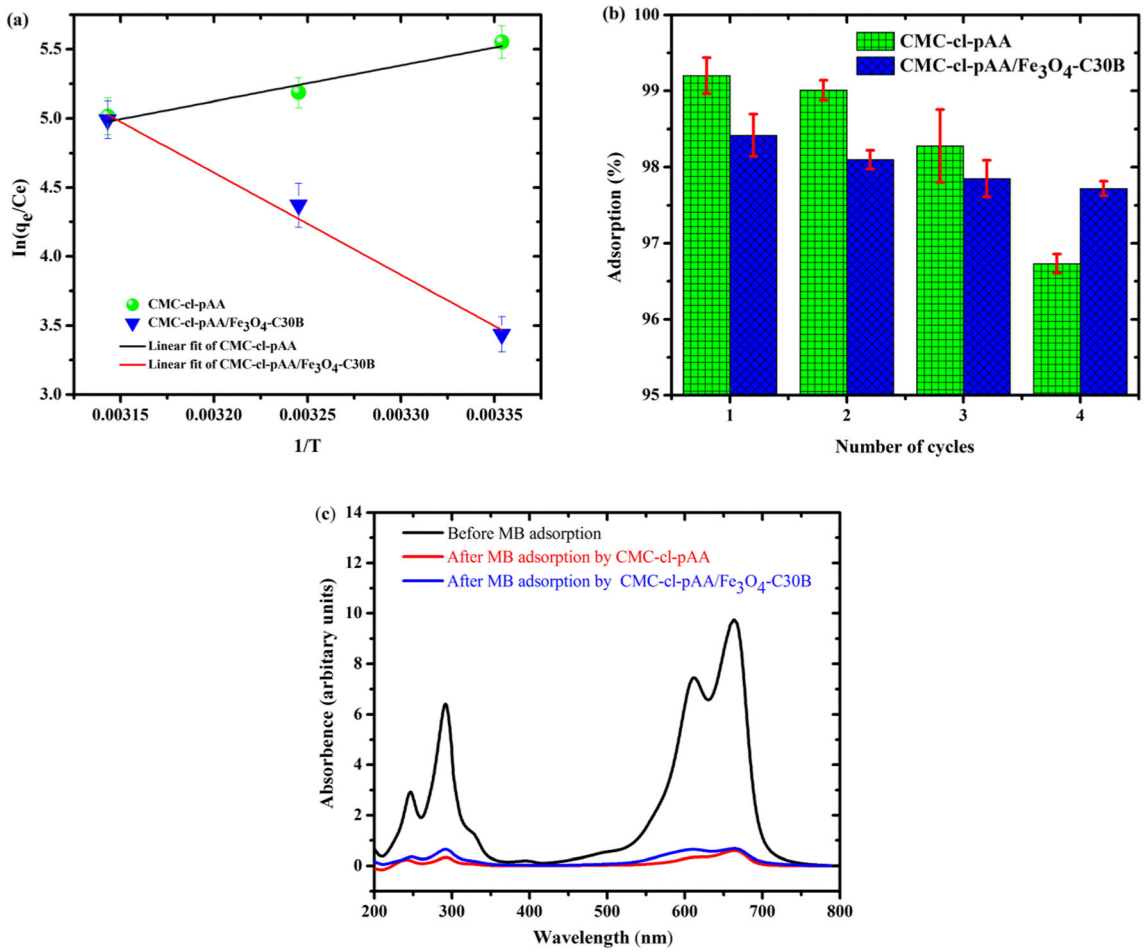

Fig. 8 **a** Plot of ln (q_e/C_e) vs 1/T. **b** Regeneration of CMC-cl-pAA hydrogel and CMC-cl-pAA/Fe_3O_4-C30B hydrogel nanocomposite for adsorption of MB. **c** UV-vis spectra of MB before as well as after adsorption by CMC-cl-pAA hydrogel and CMC-cl-pAA/Fe_3O_4-C30B hydrogel nanocomposite

it is interesting to note that the CMC-cl-pAA/Fe_3O_4-C30B hydrogel nanocomposite was able to adsorb the MB dye through an external magnetic field. Thus, CMC-cl-pAA/Fe_3O_4-C30B hydrogel nanocomposite holds a greater potential for remediation of dyes in aqueous solutions. Figure 8c shows the UV-vis absorption spectra of MB solution before adsorption and after adsorption onto CMC-cl-pAA hydrogel and CMC-cl-pAA/Fe_3O_4-C30B hydrogel nanocomposite under optimum conditions. The UV-vis absorption spectrum of MB in the solution shows four characteristic peaks at 246, 292, 613, and 662 nm. The spectra of MB after the adsorption under optimum conditions is presented in Fig. 8c. The absorbance intensity of MB after the adsorption decreased drastically without any shift of the wavelength, indicating that the adsorption was unique.

Plausible adsorption mechanism

It is well-established that the adsorption surface characteristic plays a vital role in the adsorption process (Thakur et al. 2016). Both CMC-cl-pAA hydrogel and CMC-cl-pAA/Fe_3O_4-C30B hydrogel nanocomposite contain hydrophilic functional groups on their surface (Scheme 1). These functional groups play a significant role in adsorption process. The adsorption studies through factors such as pH, dose, contact time, concentration, and temperature demonstrated that the adsorption between synthesized adsorbents and MB dye depended mainly on the changing pH values. In acidic medium, the adsorption of MB was not favourable because the carboxylic groups on the surface of the adsorbents were protonated. At high pH, the carboxylic groups on the surface of adsorbents were completely ionized as a result of a strong electrostatic interaction between anionic adsorbents and cationic MB dye. This result suggests a strong electrostatic attraction between the adsorbent and the MB dye molecules as the driving force. Furthermore, the adsorption capacity of MB for the CMC-cl-pAA/Fe_3O_4-C30B hydrogel nanocomposite was observed to be comparatively lower than that of the hydrogel. This could be due to the incorporation of Fe_3O_4-C30B nanocomposite, which could promote more cross-linking networks in the polymer matrix, leading to a decline in the number of active hydrophilic functional groups.

Conclusions

In this study, CMC-cl-pAA hydrogel and CMC-cl-pAA/Fe_3O_4-C30B hydrogel nanocomposite were successfully synthesized and characterized using various analytical techniques. Several properties, as well as the adsorptive performance of as-synthesized materials, were assessed and compared. Based on physicochemical characterization of CMC-cl-pAA hydrogel and CMC-cl-pAA/Fe_3O_4-C30B hydrogel nanocomposite, we confirmed that the incorporation of Fe_3O_4-C30B nanocomposite on the bare hydrogel improved its thermal stability and mechanical strength. Furthermore, under optimized conditions, the CMC-cl-pAA/Fe_3O_4-C30B hydrogel nanocomposite exhibited comparatively lower adsorption capacity towards MB dye than the CMC-cl-pAA hydrogel. Both adsorbents followed the pseudo-second-order and Langmuir adsorption models, indicating that the chemisorption is the controlling mechanism. The maximum adsorption capacities obtained for CMC-cl-pAA hydrogel and CMC-cl-pAA/Fe_3O_4-C30B hydrogel nanocomposite were 1109.55 and 1081.60 mg/g, respectively. The higher adsorption capacities of hydrogel and hydrogel nanocomposite could be due to the copious availability of hydrophilic functional groups on their surface. Although the CMC-cl-pAA hydrogel exhibited a higher adsorption capacity than CMC-cl-pAA/Fe_3O_4-C30B hydrogel nanocomposite, it is worth mentioning that CMC-cl-pAA/Fe_3O_4-C30B hydrogel nanocomposite offers easy separation after adsorption, reusability, and mechanical and thermal stability, which holds a greater advantage for the practical application on actual industrial wastewater.

Acknowledgements M.J. Hato is grateful to the Sasol Inzalo Foundation of South Africa for procuring both STA and UV-vis instruments.

Funding information This research was supported by the National Research Foundation (NRF) under the Thuthuka programme (UIDs. 117727, and 118113), NRF postdoctoral fellowship (UID. 116679), and University of Limpopo (Q313, R202, R232, R355), South Africa.

Compliance with ethical standards

Conflict of interest The authors declare that they have no competing interests.

References

Abreu AS, Oliveira M, Machado AV (2015) Effect of clay mineral addition on properties of bio-based polymer blends. Appl Clay Sci 104: 277–285

Acp CMC, Tooth V, Caries D, Chen Z, Cao S, Wang H, Deng X (2015) Remineralization of demineralized dentine using scaffold of CMC/ACP nanocomplexes in an in vitro tooth model of deep caries. PLoS One 10:e0116553

Adegoke KA, Bello OS (2015) Dye sequestration using agricultural wastes as adsorbents. Water Resources and Industry 12:8–24

Atta A, Akl MA, Youssef AM, Ibraheim MA (2013) Superparamagnetic core-shell polymeric nanocomposites for efficient removal of methylene blue from aqueous solutions. Adsorpt Sci Technol 31:397–419

Bao Y, Ma J, Li N (2011) Synthesis and swelling behaviours of sodium carboxymethyl cellulose-g-poly(AA-co-AM-co-AMPS)/MMT superabsorbent hydrogel. Carbohydr Polym 84:76–82

Benhalima T, Ferfera-Harrar H, Lerari D (2017) Optimization of carboxymethyl cellulose hydrogels beads generated by an anionic surfactant micelle templating for cationic dye uptake: swelling, sorption and reusability studies. Int J Biol Macromol 105:1025–1042

Boumediene M, Benaïssa H, George B, Molina S, Merlin A (2018) Effects of pH and ionic strength on methylene blue removal from synthetic aqueous solutions by sorption onto an orange peel and desorp tion study. J Mater Environ Sci 9:1700–1711

Capanema NSV, Mansur AAP, Mansur HS, de Jesus AC, Carvalho SM, Chagas P, de Oliveira LC (2018) Eco-friendly and biocompatible cross-linked carboxymethylcellulose hydrogels as adsorbents for the removal of organic dye pollutants for environmental applications. Environ Technol 39:2856–2872

Cheng J, Shi L, Lu J (2016) Amino ionic liquids-modified magnetic core/shell nanocomposite as an efficient adsorbent for dye removal. J Ind Eng Chem 36:206–214

Chin SF, Iyer KS, Raston CL (2008) Fabrication of carbon-nanotubes decorated with ultra-fine super magnetic nano-particles under continuous flow conditions. RSC, Lab Chip 8:439–442

Dai H, Huang Y, Huang H (2018) Eco-friendly polyvinyl alcohol/carboxymethyl cellulose hydrogels reinforced with graphene oxide and bentonite for enhanced adsorption of methylene blue. Carbohydr Polym 185:1–11

De Gisi S, Lofrano G, Grassi M, Notarnicola M (2016) Characteristics and adsorption capacities of low-cost sorbents for wastewater treatment: a review. Sustain Mater Technol 9:10–40

Deen GR, Chua V (2015) Synthesis and properties of new "stimuli" responsive nanocomposite hydrogels containing silver nanoparticles. Gels 1:117–134

Dogan M, Karaoglu MH, Alkan M (2009) Adsorption kinetics of maxilon yellow 4GL and maxilon red GRL dyes on kaolinite. J Hazard Mater 165:1142–1151

Fekete T, Borsa J, Takács E, Wojnárovits L (2016) Synthesis of cellulose-based superabsorbent hydrogels by high-energy irradiation in the presence of a crosslinking agent. Radiat Phys Chem 118:114–119

Gao H, Rao J, Guan YW, Li W, Zhang M, Shu T, Lv Z (2018) Investigation of the thermo-mechanical properties of blend films based on hemicelluloses and cellulose. International Journal of Polymer Science 2018:1–10

Geçgel U, Üner O, Gökara G, Bayrak Y (2016) Adsorption of cationic dyes on activated carbon obtained from waste Elaeagnus stone. Adsorpt Sci Technol 34:512–525

Godiya CB, Cheng X, Li D, Chen Z, Lu X (2018) Carboxymethyl cellulose/polyacrylamide composite hydrogel for cascaded treatment/reuse of heavy metal ions in wastewater carboxymethyl cellulose/polyacrylamide composite hydrogel for cascaded treatment/reuse of heavy metal ions in wastewater. J Hazard Mater 364:28–38

Hato MJ, Sinha Ray S, Luyt AS (2008) Nanocomposites based on polyethylene and polyhedral oligomeric silsesquioxanes, 1-microstructure, thermal and thermomechanical properties. Macromol Mater Eng 293:752–762

Hato MJ, Zhang K, Ray SS, Choi HJ (2011) Rheology of organoclay suspension. Colloid Polym Sci 289:1119–1125

Hoffman AS (2012) Hydrogels for biomedical applications. Adv Drug Deliv Rev 64:18–23

Hosseinzadeh H, Khoshnood N (2016) Removal of cationic dyes by poly (AA-co-AMPS)/montmorillonite nanocomposite hydrogel. Desalin Water Treat 57:1–12

Hu X-S, Liang R, Sun G (2018) Super-adsorbent hydrogel for removal of methylene blue dye from aqueous solution. J Mater Chem A 6: 17612–17624

Khedmat S, Momen-Heravi F, Pishvaei M (2013) A comparison of viscoelastic properties of three root canal sealers. J Dent 10:147–154

Kono H (2014) Characterization and properties of carboxymethyl cellulose hydrogels crosslinked by polyethylene glycol. Carbohydr Polym 106:84–93

Li X, Rombouts W, van der Gucht J, de Vries J, Dijksman JA (2019) Mechanics of composite hydrogels approaching phase separation. PLoS One 14:e0211059

Lin O, Gao M, Chang J, Ma H (2017) Highly effective adsorption performance of carboxymethyl cellulose microspheres crosslinked with epichlorohydrin. J Appl Polym Sci 134:44363

Liu C, Zhou Y, Nie W, Song L, Chen P (2015) Fabrication of hydrogel of hydroxypropyl cellulose (HPC) composited with graphene oxide and its application for methylene blue removal. J Mater Sci 50: 6113–6123

Liu C, Omer AM, Ouyang X (2018) Adsorptive removal of cationic methylene blue dye using carboxymethyl cellulose/k-carrageenan/activated montmorillonite composite beads: isotherm and kinetic studies. Int J Biol Macromol 106:823–833

Loh KS, Lee YH, Musa A, Salmah AA, Zamri I (2008) Use of Fe_3O_4 nanoparticles for enhancement of biosensor response to the herbicide 2,4-dichlorophenoxyacetic acid. Sensors 8:5775–5791

Magdy A, Fouad YO, Abdel-Aziz MH, Konsowa AH (2017) Synthesis and characterization of Fe_3O_4/kaolin magnetic nanocomposite and its application in wastewater treatment. J Ind Eng Chem 56:299–311

Mahdavinia G, Afzali A, Etemadi H, Hosseinzadeh H (2017) Magnetic/pH-sensitive nanocomposite hydrogel based carboxymethyl cellulose-g-polyacrylamide/montmorillonite for colon targeted drug delivery. Nanomed Res J 2:111–122

Mahmoodi NM, Hayati B, Arami M (2012) Kinetic, equilibrium and thermodynamic studies of ternary system dye removal using a biopolymer. Ind Crop Prod 35:295–301

Makhado E, Ray SS (2015) Mechanical, Barrier and antimicrobial properties of biodegradable poly (ε-caprolactone) nanocomposites. Advanced Science, Engineering and Medicine 7:351–360

Makhado E, Pandey S, Nomngongo PN, Ramontja J (2018a) Preparation and characterization of xanthan gum-cl-poly (acrylic acid)/o-MWCNTs hydrogel nanocomposite as a highly effective reusable adsorbent for removal of methylene blue from aqueous solutions. J Colloid Interface Sci 513:700–714

Makhado E, Pandey S, Ramontja J (2018b) Microwave-assisted synthesis of xanthan gum-cl-poly (acrylic acid) based-reduced graphene oxide hydrogel composite for adsorption of methylene blue and methyl violet from aqueous solution. Int J Biol Macromol 119:255–269

Makhado E, Pandey S, Kang K, Fosso-Kanke E (2019a) Microwave-assisted synthesis of xanthan gum-cl-dimethyl acrylamide hydrogel-based silica hydrogel as adsorbent for cadmium (II) removal. Int'l Conference on Science, Engineering, Technology & Waste Management (SETWM-19), 1, 1–6

Makhado E, Pandey S, Nomngongo PN, Ramontja J (2019b) New horizons in wastewaters management: emerging monitoring and remediation. Hydrogel Nanocomposites: Innovations in Nanotechnology for Water Treatment, Nova Science Publishers, (Chapter 5).

Makhado E, Pandey S, Ramontja J (2019c) Microwave-assisted green synthesis of xanthan gum grafted diethylamino ethyl methacrylate: efficient adsorption of hexavalent chromium. Carbohydr Polym 222:114989

Makhado E, Pandey S, Modibane KD, Kang M, Hato MJ (2020) Sequestration of methylene blue dye using sodium alginate poly (acrylic acid)@ ZnO hydrogel nanocomposite: kinetic, isotherm, and thermodynamic investigations. Int J Biol Macromol 162:60–73

Maponya TC, Ramohlola KE, Kera NH, Modibane KD, Maity A, Katata-Seru LM, Hato MJ (2020) Influence of magnetic nanoparticles on modified polypyrrole/m-phenylenediamine for adsorption of Cr(VI) from aqueous solution. Polymers 12:679–695

Melo BC, Paulino FAA, Cardoso VA, Pereira AGB, Fajardo AR, Rodrigues FH (2018) Cellulose nanowhiskers improve the methylene blue adsorption capacity of chitosan-g-poly (acrylic acid) hydrogel. Carbohydr Polym 181:358–367

Mishra S, Mukul A, Sen G, Jha U (2011) (2011). Microwave-assisted synthesis of polyacrylamide grafted starch (St-g-PAM) and its applicability as flocculant for water treatment. Int J Biol Macromol 48: 106–111

Mittal H, Ray SS (2016) A study on the adsorption of methylene blue onto gum ghatti/TiO_2 nanoparticles-based hydrogel nanocomposite. Int J Biol Macromol 88:66–80

Mittal H, Parashar V, Mishra SB, Mishra AK (2014) Fe_3O_4 MNPs and gum xanthan based hydrogels nanocomposites for the efficient capture of malachite green from aqueous solution. Chem Eng J 255: 471–482

Mittal H, Kumar V, Saruchi, Ray SS (2016) Adsorption of methyl violet from aqueous solution using gum xanthan/Fe_3O_4 based nanocomposite hydrogel. Int J Biol Macromol 89:1–11

Ninan N, Muthiah M, Park IK, Elain A, Thomas S, Grohens Y (2013) Pectin/carboxymethyl cellulose/microfibrillated cellulose composite scaffolds for tissue engineering. Carbohydr Polym 98:877–885

Peng N, Hu D, Zeng J, Li Y, Liang L, Chang C (2016) Superabsorbent cellulose−clay nanocomposite hydrogels for highly efficient removal of dye in water. ACS Sustain Chem Eng 4:7217–7224

Salama A (2015) Carboxymethyl cellulose-g-poly (acrylic acid)/calcium phosphate composite as a multifunctional hydrogel material. Mater Lett 157:243–247

Salama A (2018) Preparation of CMC-g-P(SPMA) super adsorbent hydrogels: exploring their capacity for MB removal from wastewater. Int J Biol Macromol 106:940–946

Shen J, Cui C, Li J, Wang L (2018) In situ synthesis of a silver-containing superabsorbent polymer via a greener method based on carboxymethyl celluloses. Molecules 23:2483

Shi Y, Xue Z, Wang X, Wang AQ (2013) Removal of methylene blue from aqueous solution by sorption on lignocellulose-g-poly (acrylic acid)/montmorillonite three-dimensional cross-linked polymeric network hydrogels. Polym Bull 70:1163–1179

Sitthichai S, Pilapong C, Thongtem T (2015) CMC-coated Fe_3O_4 nanoparticles as new MRI probes for hepatocellular carcinoma. Appl Surf Sci 356:972–977

Soliman FM, Yang W, Guo H, Shinger ML, Idris AM, Hassan ES (2016) Preparation of carboxymethyl cellulose-g-poly (acrylic acid-2-acrylamido-2-methylpropane sulfonic acid)/attapulgite superabsorbent composite. J Polym Sci 2:11–19

Song W, Gao B, Xu X, Xing L, Han S, Dua P, Song W, Jia R (2016) Adsorption–desorption behaviour of magnetic amine/Fe3O4 functionalized biopolymer resin towards anionic dyes from wastewater. Bioresour Technol 210:123–130

Soppiranth KS, Aminabhavi TM (2002) Water transport and drug release study from a cross-linked polyacrylamide grafted guar gum hydrogel microspheres for the controlled release application. Eur J Pharm Biopharm 53:87–98

Su H, Li W, Han Y, Liu N (2018) Magnetic carboxyl functional nanoporous polymer: synthesis, characterization and its application for methylene blue adsorption. Sci Rep 8:1–8

Sulistiyo YA, Andriana N, Piluharto B, Zulfikar Z (2017) Silica gels from coal fly ash as methylene blue adsorbent: isotherm and kinetic studies. Bull Chem React Eng Catal 12:263–272

Sun X, Liu B, Jing Z, Wang H (2015) Preparation and adsorption property of xylan/poly (acrylic acid) magnetic nanocomposite hydrogel adsorbent. Carbohydr Polym 118:16–23

Thakur S, Pandey S, Arotiba OA (2016) Development of a sodium alginate-based organic/inorganic superabsorbent composite hydrogel for adsorption of methylene blue. Carbohydr Polym 153:34–46

Toor AT, Verma A, Jotshi CK, Bajpai PK, Singh V (2006) Photocatalytic degradation of Direct Yellow 12 dye using UV/TiO_2 in a shallow pond slurry reactor. Dyes Pigm 68:53–60

Wang Z, Ning A, Xie P, Gao G, Xie L, Li X (2018) Synthesis and swelling behaviours of carboxymethyl cellulose-based superabsorbent resin hybridized with graphene oxide. Carbohydr Polym 157: 48–56

Wittenberg E, Meyer A, Eggers S, Abetz V (2018) Hydrogen bonding and thermoplastic elastomers–a nice couple with temperature-adjustable mechanical properties. Royal Society of Chemistry. Soft Matter 14:2701–2711

Xu J, Zhang F, Sun J, Sheng J, Wang F, Sun M (2014) Bio and nanomaterials based on Fe_3O_4. Molecules 19:21506–21528

Yadav M, Rhee KY, Jung IH, Park SJ (2013) Eco-friendly synthesis, characterization and properties of a sodium carboxymethyl cellulose/graphene oxide nanocomposite film. Cellulose 20:687–698

Yagub MT, Sen TK, Afroze S, Ang HM (2014) Dye and its removal from aqueous solution by adsorption. Adv Colloid Interf Sci 209:172–184

Yue Y, Wang X, Wu Q, Han J (2019) Assembly of polyacrylamide-sodium alginate-based organic-inorganic hydrogel with mechanical and adsorption properties. Polymer 11:1239

Zhang G, Yi L, Deng H, Sun P (2014) Dyes adsorption using a synthetic carboxymethyl cellulose-acrylic acid adsorbent. J Environ Sci 26: 1203–1211

Zhao L, Yang S (2017) Preparation and application of carboxylated graphene oxide sponge in dye removal. Int J Environ Res Public Health 14:1301

Zhu L, Qiu J, Sakai E (2017) A high modulus hydrogel obtained from hydrogen bond reconstruction and its application in vibration damper. Royal Society of Chemistry Advances 7:43755–43763